OBSERVATION OF SUBSIDENCE AT SHINHO INDUSTRIAL COMPLEX USING PERMANENT SCATTERERS

SANG-WAN KIM and JOONG-SUN WON

Department of Earth System Sciences, Yonsei University
134 Shinchon-dong, Seodaemun-gu, Seoul, 120-749, Korea
sangwan@yonsei.ac.kr

Abstract

To detect ground subsidence, the permanent scatterer SAR interferometry is applied to the Shinho industrial complex. Eleven JERS-1 images were acquired in the study area between October 1996 and September 1998. All SAR data were co-registered to one master scene (January 8, 1998) and thus 10 interferograms were obtained in a time series. In order to determine permanent scatterers, coherence maps as well as the interferograms were generated and exploited. The coherence at the selected PSs was larger than 0.4 in a 515 sub-window and 0.5 in a 39 sub-window. Twenty-nine PSs within the reclaimed land and 8 PSs (as reference phase) outside the plant were selected for the analysis. The 29 PSs were grouped into 5 sub-groups. We removed the reference phase, which was estimated from 8 outside PSs that were considered as phases free of displacement, from the phases at PSs inside the plant. Residual phases could be interpreted as surface displacement and DEM error. The subsidence of about 40 cm was detected at group 4, while surface displacements were negligible in the rest groups.

Key Words : Shinho industrial complex, Subsidence, Permanent Scatterer

I. INTRODUCTION

Differential SAR interferometry (DInSAR) has been applied successfully to estimate subtle crustal deformation by earthquakes, volcanoes activity, and ground water flux (Massonnet *et al.*, 1993; Amelung *et al.*, 2000; Sandwell *et al.*, 2000). The permanent scatterer SAR interferometry (PSInSAR) technique has also been developed more recently and has been applied to slow, but consistent, ground subsidence monitoring (Ferretti *et al.*, 2000).

The PSInSAR is a fully operational tool for millimeter-scale accuracy ground deformation mapping on a dense grid of phase stable radar targets (so-called Permanent Scatterers; PS). On the sparse grid of PS, the various contribution to the differential interferometric phase (residual topography due to inaccuracies in the reference DEM, ground deformation, atmospheric signature and noise) can be discriminated. But there are difficulties in phase unwrapping on the sparse grid if the phase change from one permanent scatterer (PS) to the neighboring PS is larger than a factor of (Ferretti *et al.*, 2000). In this paper we apply the permanent scatterer SAR interferometry to the Shinho industrial complex in which the Samsung-Renault Automobile plant was built on a reclaimed coastal land.

II. PS SELECTION

For the study, we used eleven JERS-1 SAR images acquired between October 25 1996 and September 29 1998. Table 1 lists the JERS-1 SAR data sets used, the time spanning of the interferometric pairs, and their corresponding the altitude of ambiguity. We selected a data set acquired January 8, 1998 as a master image based on temporal and geometrical baselines of each possible pair. All were resampled on the master data and 10 interferograms were obtained in a time series.

In order to identify stable targets, the coherence maps associated with the interferograms were used. Correlation thresholding would be the easiest approach. If a target exhibits a coherence always greater than a certain value, that can be selected as a PS candidate. The two variables to be optimized are the coherence threshold and the dimension of the sub-window. The larger the window dimension is, the higher the estimator accuracy is but trading

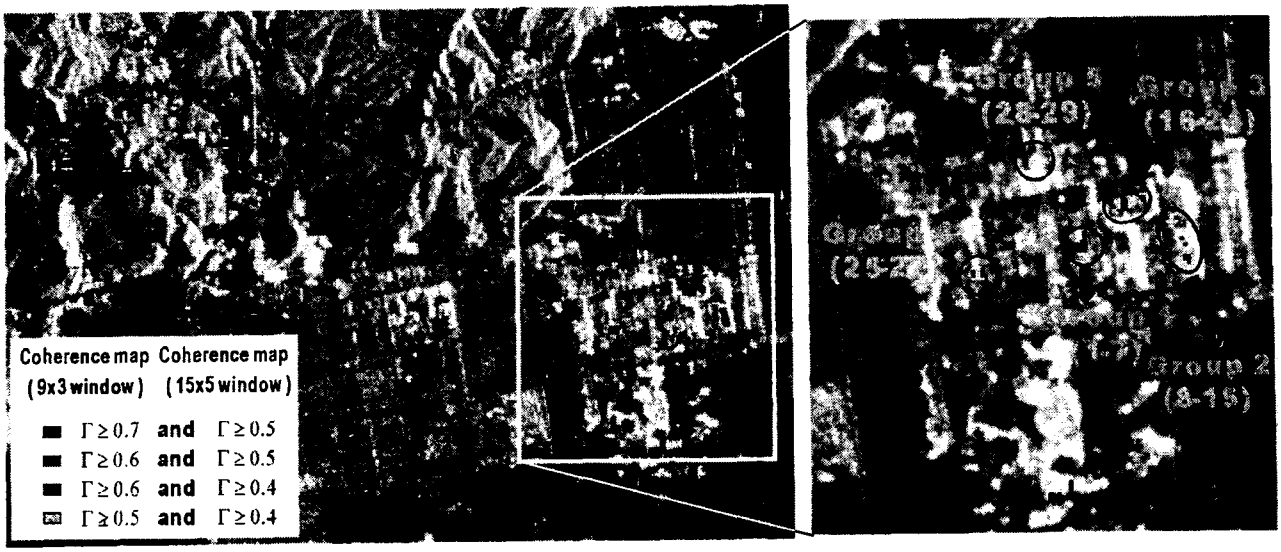

Figure 1. The location map of the reference PS and PS selected inside the Renault-Samsung automobile company.

off the detection probability. In fact, many stable targets surrounded by noncoherent clutter are lost when large estimation windows are used. Similar considerations hold for coherence thresholding. Window dimension and coherence threshold are the result of a tradeoff between estimator accuracy and detection probability. The new strategy has been developed to select PS through analyzing the time series of the amplitude values of each pixel (Ferretti *et al.*, 2001). The method can be adopted when many SAR images (> 30) are available and they must be radiometrically corrected. But data used were not enough to fulfill these conditions, thus this method could not be applied in this study.

Here two sub-windows with different size were used to select a precise pixel with high estimator accuracy. The coherence at the selected PSs was larger than 0.4 in a 515 sub-window and 0.5 in a 39 sub-window. Eight PSs, which are supposedly stable, outside the plant were selected for the analysis of reference phase. PS1-PS4 are located near the study area and have a similar elevation, thus atmospheric distortions and DEM error could be minimized. On the other hand PS5-PS8 far from the study area were selected to verify the accuracy of baseline estimation. Twenty-nine PSs within the reclaimed land were selected for the subsidence analysis. The 29 PSs were grouped into 5 sub-groups (Figure 1).

Table 1. Summary of the JERS-1 SAR images used.

No.	Date	Perpendicular baseline (m)	Time interval (day)
1	96/10/25	1260.0	-440
2	97/01/21	1744.3	-352
3	97/06/02	1521.8	-220
4	97/10/12	2041.9	-88
5	97/11/25	592.5	-44
6	98/01/08	0	0
7	98/02/21	457.7	44
8	96/05/02	1820.4	132
9	98/07/03	620.3	176
10	98/08/16	176.9	220
11	98/09/29	855.3	264

III. DIFFERENTIAL PROCESSING

Given a reference phase (θ_{ref}) and height (H_{ref}) and a PS height (H_{ps}), the surface displacement ($\triangle z$) can be estimated through simple arithmetic operation of the following equations:

$$e^{i\theta_d} = e^{i\theta_{ref}} \cdot e^{i\frac{H_{ps}-H_{ref}}{h_a}2\pi} \cdot e^{-i\theta_{ps}}, \quad (1)$$

$$\triangle z = \frac{\lambda \theta_d}{4\pi \cos(\theta_{inc})}. \quad (2)$$

Where λ is a wavelength of SAR signal, and θ_{inc} is an incidence angle.

Figure 2 shows phase values of eight reference PSs in each interferometric pair. The circle and asterisk respectively denote simple phase difference and differential phase after height correction using

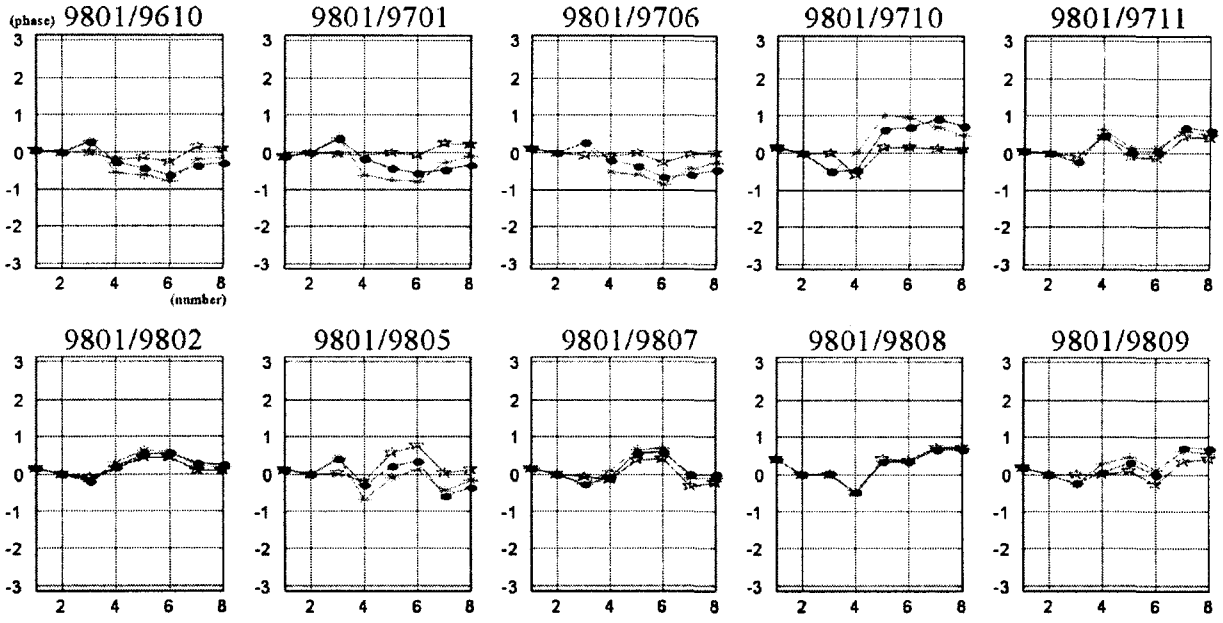

Figure 2. Differential phase of the reference PS.

equation (1) and (2) with respect to PS2. The DEM was estimated from a tandem pairs of the ERS-1/2 data sets acquired in December 1995. The perpendicular baseline of the ERS-1/2 tandem pair was at -315.4 m and yielded a -25.8 m altitude of ambiguity. Therefore the accuracy of DEM would be high (~10 m) in smooth terrain. Its accuracy is not an obstacle(20 m is enough). In fact, DEM refinement (in correspondence to the PS) is carried out using procedure presented in the following paragraph.

Differential phase data (ϕ_i) are the sum of four contributions (Ferretti *et al.*, 2000):

$$\phi_i = \frac{4\pi}{\lambda} \Delta\rho_i + \alpha_i + n_i + t_i, \qquad (3)$$

where

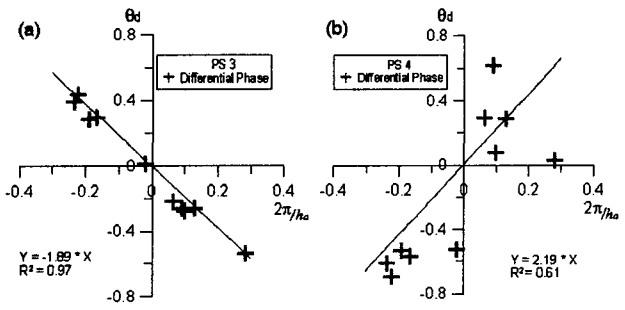

Figure 3. Relation of h_a and differential phase for the DEM error correction. (a) PS 3, (b) PS 4.

$\Delta\rho_i$ motion of the target projected on the line of sight (LOS);

α_i phase due to atmospheric distortions;

n_i decorrelation noise;

t_i phase due to DEM errors.

Basically, one has to carry out a joint estimation of DEM errors, LOS velocities, and atmospheric contributions. Here we can ignore atmospheric effect since the study area is very small (about 1.51 km). We used the following method to simply the problem. Substituting $H_{ps} + \varepsilon_h$ for H_{ps} in equation (1), phase error (t_i) induced by ε_h is then given by

$$t_i = \varepsilon_h \cdot \frac{2\pi}{h_a} . \qquad (4)$$

Thus DEM errors can be easily detected from the linear relationship between residual differential phase and $2\pi/h_a$. For example, Figure 3 shows the result of PS3 and PS4. Most residual phases can be considered as DEM errors in Figure 3a, while residual phases unrelated to DEM errors exist in Figure 3b. They may be caused by additional errors such as decorrelation noises or atmospheric artifacts. Phase errors can be removed by subtracting phase induced by DEM error, which corresponds the

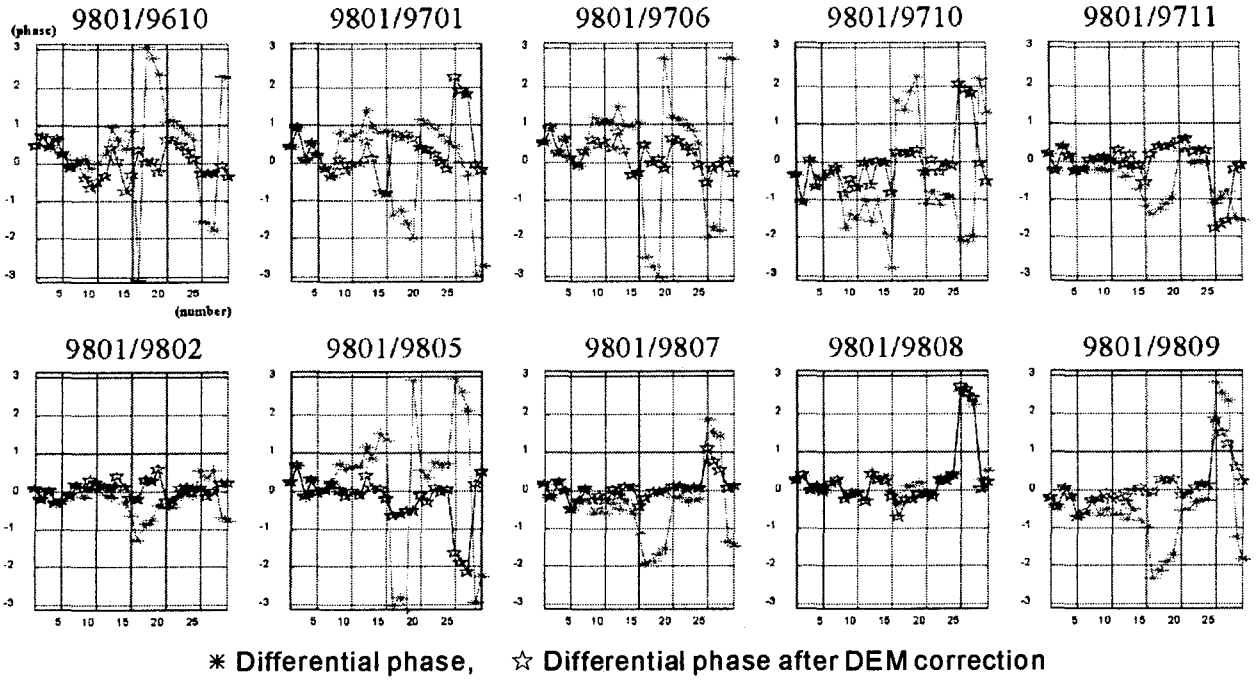

Figure 4. Differential phase of PS inside the study area.

regression line gradient in Figure 3. After DEM correction, differential phase values is closer to zero (Figure 2).

We removed the reference phase, which was estimated from 8 outside PSs and could be considered as phases unrelated to displacement, from the phases at PSs in the plant. Residual phases could be interpreted as surface displacement and DEM error. Finally, DEM refinement was carried out to have result in Figure 4.

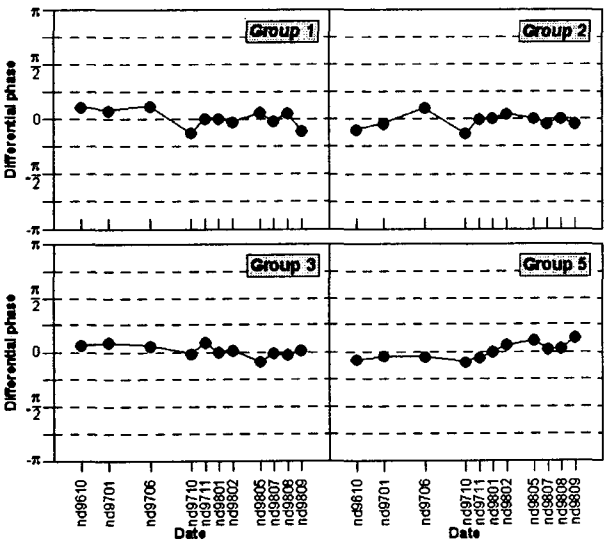

Figure 5. Differential phase of the non-deformation group.

IV. RESULTS AND CONCLUSIONS

The mean phase of each group was calculated and then it is plotted with acquisition time of slave data. The phase variation is not detected in group 1, group 2, group 3, and group 5 (Figure 5). In other words, surface displacements are not observable in these groups. However, we observed phase variation clearly in group 4 (Figure 6). The phase was unwrapped, and then converted to surface displacements. As a result, the subsidence of about 40 cm along LOS was detected at group 4. If the estimated LOS displacement is projected in vertical

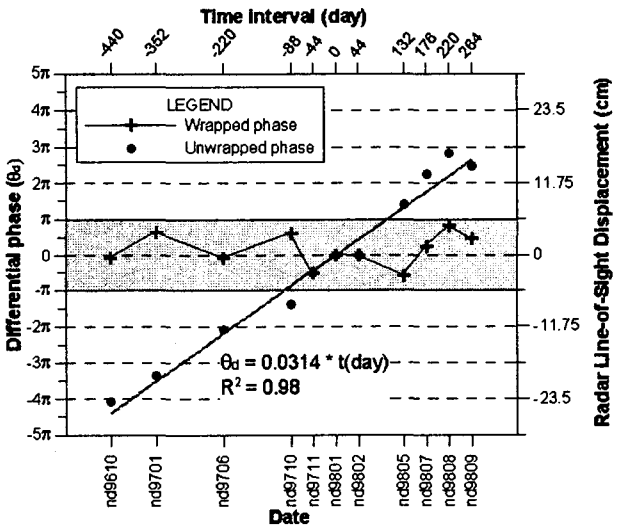

Figure 6. Total differential phase of the group 4.

plane, the amount of subsidence is about 54 cm.

The PSs might represent different mechanism. PSs in group 1, 2, 3, 5 might be backscattering from top of buildings and only group 4 corresponds to a corner scattering from ground surface. In the study area buildings are known to be stable, thus the phase of only group 4 can reveal ground displacements. Although verification of these results was not carried out because in-situ measurement was not available, they were confirmed by personal communication.

REFERENCES

A. Ferretti, C. Prati, and F. Rocca, 2001, Permanent Scatterers in SAR Interferometry, *IEEE Trans. Geosci. Remote Sensing*, 39(1): 8-20.

A. Ferretti, C. Prati, and F. Rocca, 2000, Nonlinear subsidence rate estimation using permanent scatterers in Differential SAR Interferometry, *IEEE Trans. Geosci. Remote Sensing*, 38(5): 2202-2211.

D. Massonnet, M. Rossi, C. Carmona, F. Adragna, G. Peltzer, K. Fiegl and T. Rabaute, 1993. The displacement field of the Landers earthquake mapped by radar interferometry, *Nature*, 364: 138-142.

D.T. Sandwell, L. Sichoix, D. Agnew, Y. Bock, and J-B. Minster, 2000, Near real-time radar interferometry of the Mw 7.1 Hector Mine Earthquake, *Geophys. Res. Lett.*, 27(19): 3101-3104.

F. Amelung, D. L. Galloway, J. W. Bell, H. A. Zebker, and R. J. Laczniak, 1999, Sensing the ups and downs of Las Vegas: InSAR reveals structural control of land subsidence and aquifersystem deformation, *Geology*, 27(6): 483-486.